High-Efficiency Wearable Wireless Power Transfer using Magnetoinductive Waveguides

Connor Jenkins and Asimina Kiourti

ElectroScience Laboratory, Department of Electrical and Computer Engineering, The Ohio State University, Columbus, OH 43212 USA (email: jenkins.1124@osu.edu)

***Abstract*— We report a new method for high-efficiency wireless power transfer in wearable applications based upon the concept of alternately coupled magnetoinductive waveguides (MIWs). MIWs are formed by a series of coupled electrically small resonant loops. By carefully manipulating the phase of alternately coupled elements, the reported approach reduces the impacts of constructive and destructive interference introduced by the termination of the MIW. This allows for a steady performance across the entire length rather than the large nulls and maximums seen in a typical design. A proof-of-concept design is provided and validated numerically and *in vivo*. Our approach improves upon the state-of-the-art in terms of both maximum transmission distance (75 cm versus <10 cm) and wireless power transfer efficiency (49% versus <30%), while maintaining robustness to a variety of non-idealities.**

I. Introduction

As the use of wearables and implants increases in a variety of applications, the need to unobtrusively power or charge these devices becomes paramount. With this in mind, there is an increased interest in wearable wireless power transfer (WPT) that allows power to flow unobtrusively from either an on-body or external power source to one or more on-body devices. While WPT in free space is a well-studied area [1], creating a wearable system introduces several challenges: 1) effects of human tissue energy absorption on performance and safety, 2) space limitations due to human anatomy, and 3) design limitations due to wearability requirements.

The primary technologies used for wearable WPT are human body communications (HBC), magnetic induction (MI) and magnetic resonant coupling (MRC), Table I. HBC utilizes capacitive coupling between two electrodes worn on the body, set up such that the forward path is through the human tissue while the return path couples to the outside environment [2]. These designs allow for the free placement of devices relative to the power source but are extremely limited in efficiency (~14%) and range (~16 cm) due to the large losses in the human tissue [2]. MI relies on Faraday's Law to couple a transmit and receive coil and transfer power between them [3]. While power is not lost in excess in the human body, MI is still limited in range (as power transfer falls off rapidly with distance), practical applicability (as it requires strong alignment), and efficiency (~30%) [3]. Finally, MRC follows directly from the MI technology with the transmit and receive elements made resonant at the same frequency. Though MRC allows for increased range (~10 cm) and efficiency (64%) versus MI [4], it still does not solve the alignment problems, as the misalignment losses remain significant in practice.

TABLE I. COMPARISON OF WEARABLE WIRELESS POWER TRANSFER TECHNOLOGIES

Technology	Path Loss	Efficiency	Transmit Range	Device Placement
HBC	High	Low	Medium	Variable
MI	Low	Medium	Low	Fixed
MRC	Low	High	Low	Fixed
AC-MIW (Proposed)	**Extremely Low**	**Medium**	**Extremely Large**	**Variable**

In this work, we introduce magnetoinductive waveguides (MIWs) as a new technology for use in wearable WPT systems that overcomes the limitations in receiver placement of MI and MRC while maintaining high levels of power transfer efficiency and dramatically increased range. MIWs are a transmission-line-like structure formed by a series of coupled electrically small resonant elements. Through Faraday's Law and careful design, a current excited on an element leads to a traveling wave across the structure that can be used for communication, wireless body area networks, or WPT [5]-[7].

MIW studies for WPT have so far been limited to free space applications [7]. In a major leap forward, we explore a novel MIW approach for WPT in wearable applications. To utilize the open structure of the MIW most effectively, we focus on the transfer of power to a transducer placed anywhere along the length of the MIW. This setup allows for variable device placement without sacrificing performance and without requiring a new design for each unique device placement. With this in mind, there are two main challenges that must be overcome: 1) reflections introduced by the presence of the transducer and 2) standing wave effects introduced by terminating the MIW. Problem 1) is solved by careful manipulation of the mutual coupling between the transducer and each element of the MIW and the load impedance of the transducer itself [7]. For Problem 2), we utilize an alternately coupled MIW (AC-MIW) design [7].

The remainder of the paper is setup as follows: Section II discusses the MIW operating principle, Section III covers the AC-MIW and transducer design requirements and principles, Section IV shows ideal simulated and experimental results while Section V handles real-world concerns for wearable WPT. The paper concludes in Section VI.

II. Operating Principle

The primary challenge with using MIWs for WPT lies in controlling the standing wave effects introduced by terminating the MIW. As with a traditional transmission line, when an MIW is terminated with a load not equal to its characteristic

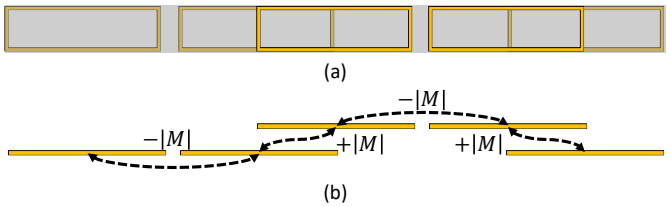

Figure 1. Model of AC-MIW: a) top view and b) side view with labeled coupling polarities.

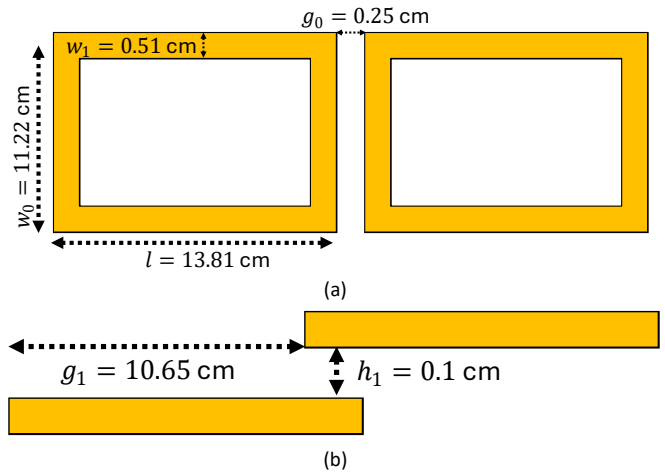

Figure 2. Dimensions of AC-MIW design: a) negative coupling polarity geometry and b) positive coupling polarity geometry.

impedance (Z_0), some of the incoming wave is reflected, leading to both constructive and destructive interference along the length of the MIW [7]. For a monoatomic MIW operating at resonance, the interference alternates between each element due to the $\pm\pi/2$ phase progression incurred with each element [5]. This interference leads to inconsistent magnetic field strength and inconsistent power transfer efficiency (PTE) across the length of the MIW, which is undesirable. The first-order solution is to terminate the MIW with a load equal to the characteristic impedance of the MIW, but, doing so, halves the maximum PTE and makes the solution ineffective [7].

The state-of-the-art solution relies on manipulating the phase of the incident and reflected wave by utilizing a specific termination impedance and an alternately coupled design, Fig. 1. By terminating the MIW with $\pm jZ_0$ and alternating the coupling polarity between adjacent elements (here referring to the sign of the mutual inductance between elements), the incident and reflected waves are always out of phase by $\pm\pi/2$ depending on the sign of the terminating impedance. This leads to consistent destructive interference across the entire length of the MIW, thus reducing the maximum PTE, but greatly increasing the average PTE. In this work, we extend this design approach to the wearable scenario.

III. Alternately Coupled MIW and Transducer Design

A. AC-MIW Design

The first step to designing an MIW is to determine the element geometry. Because we are only interested in single-frequency operation for WPT, our MIW element design relies solely on reducing the propagation loss across the length of the MIW. The first-order dispersion relation for a lossy uniform monoatomic MIW with geometric periodicity, p, is

$$-\frac{j}{Q}+1-\frac{\omega_0^2}{\omega^2}+\kappa\cos(\gamma p)=0 \qquad (1)$$

where the self- impedance of each loop is identical at $Z=R+j\omega L+1/j\omega C$ and each loop is coupled to its nearest neighbor with mutual inductance M such that $Q=\omega L/R$, $\kappa=2M/L$, $\omega_0=1/\sqrt{LC}$. This leads to a complex propagation constant $\gamma=\beta-j\alpha$, where β is the phase constant and α is the attenuation constant. When operating at resonance, we can approximate the total loss along an N-unit MIW following the form of Eq. (1) as $N\alpha p$. This can then be minimized for a given MIW length, Np, via element design. For the free-space case, this would be sufficient; but because this is a wearable system, we have a number of other limitations.

First, to create the wearable system we rely on embroidery techniques with e-threads. Without loss of generality, we select Liberator-40 e-threads that have a conductivity of ~7.33×10^6 S/m [6] and enforce a minimum feature size of ~0.25 cm. We also utilize felt fabrics that are 0.1 cm thick for ease of fabrication and user comfort. Second, we must ensure that the elements can fit across the entirety of the typical human body. With this in mind, we limit our element size to a maximum dimension of ~14 cm, representing a very small wrist circumference [8]. Finally, we limit our geometry to single turn, rectangular loops for this proof-of-concept result, noting that multi-turn loops and other geometries may lead to significant performance improvements in the future. With these limitations in mind, we target an operating frequency of 13.56 MHz, which enables us to operate in the electrically small region while enabling integration with off-the-shelf NFC devices.

With the constraints defined, we model two identical elements, as shown in Fig. 2, at a distance of $g_0=0.25$ cm and varying l, w_0, and w_1. The geometry is optimized in CST Studio [9] to minimize propagation loss, and the final element dimensions are found to be $l=13.81, w_0=11.22$, and $w_1=0.51$ cm, leading to $Q=55$ and $\kappa=0.19$. With the negative coupling geometry set, we select h_1 as 0.1 cm to represent a typical fabric thickness and set $g_1=10.65$ cm to achieve the required mutual inductance of 31.65 nH for the positive polarity geometry shown in Fig. 2. With this design set, we have a characteristic impedance at the resonant frequency of $Z_0=\omega_0 M=2.7\ \Omega$.

B. Transducer Design

Because the transducer can be placed over any position along the length of the MIW, we must ensure that the effective impedance inserted into the MIW by the presence of the transducer is equal to the characteristic impedance of the MIW such that no reflections are introduced. This is a function of the geometry of the transducer, the geometry of the MIW, and the load impedance placed on the transducer as governed by [7]

$$R_L=\frac{\omega_0 M_t^2}{Me^{-\alpha p}}-R_t \qquad (2)$$

where R_L is the load impedance on the transducer, and M_t and R_t are the mutual inductance between the transducer and element, and the resistance of the transducer, respectively.

Since the design is wearable, the distance between the MIW and the transducer is determined by the thickness of the fabric the transducer is created on. For example, we can

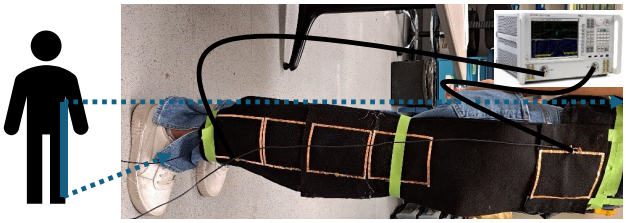

Figure 3. Human subject AC-MIW experimental setup.

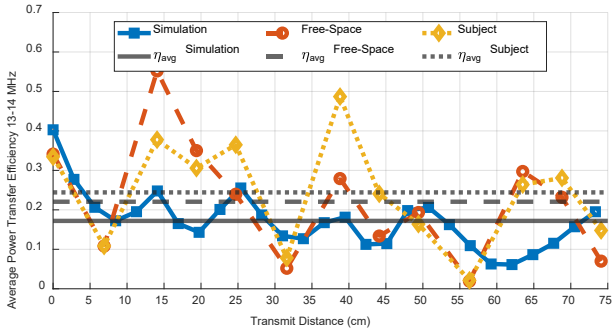

Figure 4. PTE for simulation, free space, and *in vivo* measurements.

envision a lightweight device mounted via a fabric-based quick-attach mechanism, such as Velcro. With this in mind, we set our transducer height to 0.5 cm, corresponding to the approximate thickness of a Velcro-enabled fabric. We also select the transducer to be identical to the MIW elements as a proof-of-concept. This leads to $M_t = 222.4$ nH and, assuming losses to be small, $R_L = 146\ \Omega$.

IV. Simulated and *In Vivo* Experimental Performance

With the AC-MIW and transducer designs finalized, we now explore the performance of the wearable system in simulation and *in vivo*. For both scenarios, a 7-unit MIW is used, corresponding to a total length of approximately 75 cm.

A. Simulation Setup

The AC-MIW is modeled in CST Studio and placed 0.1 cm over a block with electrical properties equal to 2/3rds those of muscle to mimic the average human body [6]. The transducer and non-terminating elements are loaded with 422 pF capacitors to achieve resonance at 13.56 MHz, while the terminal element is loaded with a 385 pF capacitor to generate a termination impedance of $-jZ_0 = -j2.7\ \Omega$. This termination ensures proper phase manipulation for the desired reflection behavior (see Section II). The transmit element and the transducer are fed using 50 Ω ports and the PTE is calculated in post-processing using the reported $R_L = 146\ \Omega$ and $R_S = 0.75 \times Z_0 = 2.025\ \Omega$ [7].

B. Experimental Setup

For *in vivo* testing, the AC-MIW is created using copper-tape placed on fabric to mimic the eventual Liberator-40 embroidered design. To align with the retrieved circuit parameters of the simulation, g_1 is reduced to 10.5 cm, while the resonant capacitors are shifted to 376 pF and the termination capacitor is shifted to 344 pF. After fabrication, the system is tested in free-space and on a human subject (Institutional Review Board study #2020H0548), Fig. 3. The transducer is kept in place through Velcro anchor points, while the AC-MIW is attached tightly to the subject using tape. For each test point, S-Parameters are measured using a vector network analyzer with the PTE calculated in post-processing.

C. Results

To determine the system effectiveness, we first define PTE as

$$\eta = \frac{|S_{21}|^2(1-|\Gamma_L|^2)(1-|\Gamma_S|^2)}{|1-\Gamma_S\Gamma_{in}|^2|1-S_{22}\Gamma_L|^2} \quad (3)$$

where $\Gamma_L = (Z_L - Z_{ref})/(Z_L + Z_{ref})$, $\Gamma_S = (Z_S - Z_{ref})/(Z_S + Z_{ref})$, $\Gamma_{in} = S_{11} + S_{12}S_{21}\Gamma_L/(1-S_{22}\Gamma_L)$, and Z_{ref} is the reference impedance used in measurement. Because our transducer can be placed anywhere along the MIW, we take samples with the transducer at several locations and report the average, minimum and maximum (η_{avg}, η_{min}, η_{max}) PTEs over the given transmit distance. In addition, for this proof-of-concept study, rather than reporting the PTE solely at 13.56 MHz, the average from 13-14 MHz is taken for each sample to account for any fluctuations in frequency. These will be explored and minimized in future work.

Fig. 4 shows the average PTE from 13-14 MHz for the simulation and two experimental setups at several samples along the MIW length. The simulation achieves $\eta_{avg} = 17.2\%$, $\eta_{min} = 6.1\%$, and $\eta_{max} = 40.2\%$. Both experiments have marginally larger average and maximum results with the free-space setup showing $\eta_{avg} = 22.1\%$ and $\eta_{max} = 55.2\%$ and the human subject testing attaining $\eta_{avg} = 24.4\%$ and $\eta_{max} = 48.7\%$. At the same time, both experiments demonstrate slightly worse minimum PTE with $\eta_{min} = 1.9\%$ and $\eta_{min} = 2.1\%$ for the free-space and human subject experiments, respectively. In general, the agreement between the simulation and experimental results is good, but it is clear from the overall behavior over transmit distance that the reflection control was not fully achieved in the experimental setup. This explains both the higher maximums and lower minimums seen in the free-space and human subject trials.

Despite this, it is clear that our system is capable of achieving a WPT range of over 75 cm which is significantly larger than all current state-of-the-art technologies. At the same time, the PTE is similar to the highest efficiency systems, despite this increased range. In addition to the performance benefits, our system also demonstrates the ability to freely place the device anywhere along a large area, essentially eliminating misalignment loss in one dimension.

V. Real-World Considerations

With the ideal performance confirmed to out-perform the state-of-the-art wearable WPT systems in terms of PTE, transmit distance, and device placement, we look to two real-world considerations: 1) variation in tissue electrical properties and 2) transducer misalignment.

The electrical properties of human tissue can vary between individuals by as much as 20% [10]. To ensure that the proposed system can be used for a wide range of individuals, we examine the effect of a 20% change in both the relative permittivity, ϵ_r, and conductivity, σ, of tissue to the PTE of the system. We select the properties equal to two-thirds that of muscle at 13.56 MHz, with $\epsilon_r = 92.12$ and $\sigma = 0.42$ S/m.

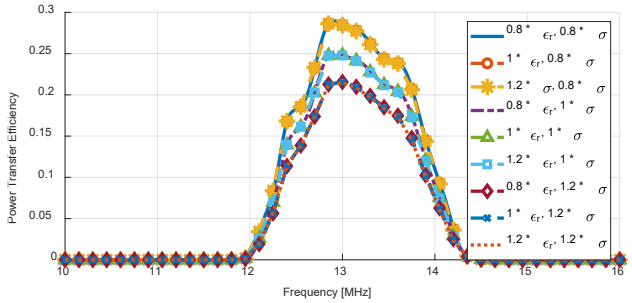

Figure 5. PTE for electrical property tissue variations of ±20%.

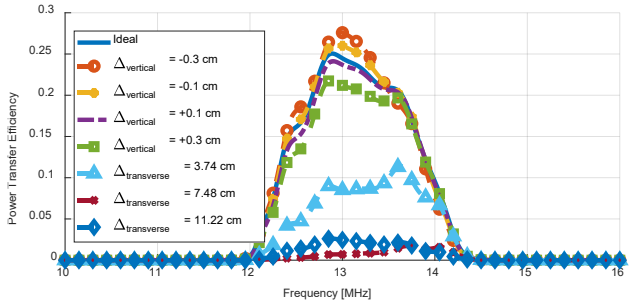

Figure 6. PTE performance with transducer misalignment.

The 20% change is then applied to these values. Fig. 5 shows the PTE over frequency for all 9 combinations of ϵ_r and σ. Overall, the performance is very stable to changes in ϵ_r and mostly stable to changes in σ. Specifically, as σ increases, PTE decreases and vice versa. This behavior is expected as the increased conductivity leads to larger loss in the tissue from coupled magnetic fields, while the changing permittivity does not have this same effect.

Next, transducer misalignment is likely to occur in this system as the devices may be placed directly by the users. As previously shown, the transducer can safely be placed anywhere along the length of the MIW while maintaining strong PTE. With this in mind, we instead examine the worst case scenario when the transducer is placed at the center of the final AC-MIW element and shifted perpendicular to the length of the MIW (transverse) or away from the tissue (vertical). The PTE over frequency for each misaligned scenario is shown in Fig. 6. For the vertical misalignment, the performance is relatively robust to change for variations up to ±0.3 cm from the target height of 0.5 cm. Because this is a wearable system, these values are reasonable when compared to thicknesses of fabric. Overall, this robustness is to be expected as the small changes in height only lead to a small change in mutual inductance between the transducer and the element. As for the transverse case, once the transducer is shifted by 1/3rd its width (3.74 cm), the PTE drops substantially; and at least 2/3rds its width (7.48 cm), it is no longer viable. This is caused by using a transducer that is identical to the AC-MIW elements such that any amount of misalignment leads to a decrease in the overlap between the AC-MIW.

VI. Conclusion

In this work, we presented a novel wearable WPT system that utilized an AC-MIW design to allow for long-range, high efficiency power transfer to wearable devices that out-performs the state-of-the-art. After optimization of both the AC-MIW and the transducer, a wearable prototype was fabricated and tested on a human subject. The system demonstrated an average and maximum PTE of 24.4% and 48.7%, respectively, over a 75 cm transmit range. In addition, simulated results indicate that the system is largely invariant to changes in tissue properties between individuals. Notably, the transducer can be freely placed anywhere along the length of the AC-MIW and shifted towards or away from the body without substantial loss of performance. However, misalignment transverse to the AC-MIW leads to significant loss of performance as attributed to the choice of transducer geometry rather than a limitation of the approach. Future work will expand upon the reported robustness studies to include additional mechanical considerations, and experimental results will also be enhanced through a better characterization of the MIW characteristic impedance to allow for a stronger reduction in the standing wave effect.

Acknowledgment

This work was supported by the National Science Foundation (NSF) under grant 20053318.

References

[1] Z. Zhang, H. Pang, A. Georgiadis, and C. Cecati, "Wireless Power Transfer—An Overview," *IEEE Trans. Ind. Electron.*, vol. 66, no. 2, pp. 1044–1058, Feb. 2019, doi: 10.1109/TIE.2018.2835378.

[2] R. Shukla, N. Kiran, R. Wang, J. Gummeson, and S. I. Lee, "SkinnyPower: enabling batteryless wearable sensors via intra-body power transfer," in *Proceedings of the 17th Conference on Embedded Networked Sensor Systems*, New York New York: ACM, Nov. 2019, pp. 68–82. doi: 10.1145/3356250.3360034.

[3] R. Lin, H.-J. Kim, S. Achavananthadith, S. A. Kurt, S. C. C. Tan, H. Yao, B. C. K. Tee, J. K. W. Lee, and J. S. Ho, "Wireless battery-free body sensor networks using near-field-enabled clothing," *Nat Commun*, vol. 11, no. 1, p. 444, Jan. 2020, doi: 10.1038/s41467-020-14311-2.

[4] M. Wagih, A. Komolafe, and B. Zaghari, "Dual-Receiver Wearable 6.78 MHz Resonant Inductive Wireless Power Transfer Glove Using Embroidered Textile Coils," *IEEE Access*, vol. 8, pp. 24630–24642, 2020, doi: 10.1109/ACCESS.2020.2971086.

[5] E. Shamonina, V. A. Kalinin, K. H. Ringhofer, and L. Solymar, "Magnetoinductive waves in one, two, and three dimensions," *Journal of Applied Physics*, vol. 92, no. 10, pp. 6252–6261, Nov. 2002, doi: 10.1063/1.1510945.

[6] C. B. Jenkins and A. Kiourti, "Wearable Dual-Layer Planar Magnetoinductive Waveguide for Wireless Body Area Networks," *IEEE Transactions on Antennas and Propagation*, vol. 71, no. 8, pp. 6893–6905, Aug. 2023, doi: 10.1109/TAP.2023.3286042.

[7] C. Rakluea, A. Worapishet, S. Chaimool, Y. Zhao, and P. Akkaraekthalin, "True Nulls-Free Magnetoinductive Waveguides Using Alternate Coupling Polarities for Batteryless Dynamic Wireless Power Transfer Applications," *IEEE Trans. Power Electron.*, vol. 37, no. 8, pp. 8835–8854, Aug. 2022, doi: 10.1109/TPEL.2022.3145579.

[8] C. Gordon, T. Churchill, C. Charles, B. Bradtmiller, J. McConville, I. Tebbetts, and R. Walker, "1988 Anthropometric Survey of U.S. Army Personnel: Methods and Summary Statistics," United States Army Natick Research, Devleopment and Engineering Center, Yellow Springs, OH, AD-A225 094, 1988.

[9] Dassault Systemes, "Electromagnetic Simulation Solvers | CST Studio Suite," Dassault Systemes. Accessed: Sep. 07, 2023. [Online]. Available: https://www.3ds.com/products-services/simulia/products/cst-studio-suite/solvers/

[10] V. Mishra and A. Kiourti, "Wearable Magnetoinductive Waveguide for Low-Loss Wireless Body Area Networks," *IEEE Trans. Antennas Propagat.*, vol. 69, no. 5, pp. 2864–2876, May 2021, doi: 10.1109/TAP.2020.3030987.